LANGMUIR Article
Cite This: Langmuir 2018, 34, 3058−3067
pubs.acs.org/Langmuir

Hyperbranched Multiarm Copolymers with a UCST Phase Transition: Topological Effect and the Mechanism

Meiwei Qi, Ke Li, Yongli Zheng, Tahir Rasheed, and Yongfeng Zhou*

School of Chemistry and Chemical Engineering, State Key Laboratory of Metal Matrix Composites, Shanghai Jiao Tong University, 800 Dongchuan Road, Shanghai 200240, China

Supporting Information

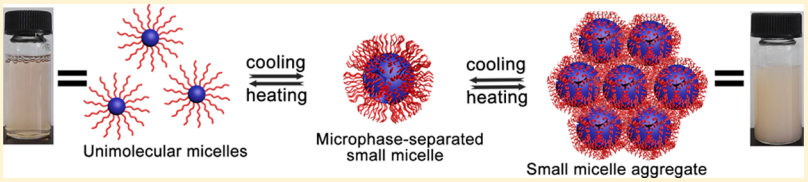

ABSTRACT: A novel thermoresponsive hyperbranched multiarm copolymer with a hydrophobic hyperbranched poly[3-ethyl-3-(hydroxymethyl)oxetane] core and many poly(acrylamide-*co*-acrylonitrile) (P(AAm-*co*-AN)) arms was for the first time synthesized through a reversible addition−fragmentation chain-transfer polymerization. These copolymers show reversible, sharp, and controlled temperature-responsive phase transitions at the upper critical solution temperature (UCST) in water and electrolyte solution. It is the first report on the hyperbranched copolymers with a UCST transition. Two series copolymers with variable AN content (series A) and variable arm length (series B) were synthesized to study the influence of molecular structure on the UCST transition. It was found that the UCST of copolymers could be raised by increasing the AN content or decreasing the arm length. Most interestingly, the amplification effect of the hyperbranched topological structure leads to a broad change of the UCST from 33.2 to 65.2 °C with the little change of AN content (5.9%). On the basis of variable temperature nuclear magnetic resonance, dynamic light scattering, and transmission electron microscopy, a UCST transition mechanism, in combination with hydrophilic/hydrophobic balance and multimicelle aggregate (MMA), was proposed. This work enriches the UCST copolymer topology and may extend the knowledge on the structure−activity relationship as well as the mechanism of the UCST polymers.

1. INTRODUCTION

Stimuli-responsive polymers have attracted considerable attention over the past few years because of their numerous so-called "smart" applications in biological and material fields.[1,2] Thermoresponsive polymers are one of the most extensively exploited intelligent materials because the temperature, as a physical stimulus, can be easily changed and controlled.[3,4] Specially, water-soluble thermoresponsive polymers have played an increasingly important role in the vast field of biochemistry and biomedicine.[5] Generally, water-soluble thermoresponsive polymers show a sharp change in properties, mainly fast and reversible phase transition from a soluble to an insoluble state, upon a small or modest change in temperature. They are divided into two types: one type displays a low critical solution temperature (LCST) in water and the phase separation from solution occurs upon heating; the other has an upper critical solution temperature (UCST) and undergoes phase separation upon cooling. As is known to all, the LCST polymers have been widely studied and applied in many fields including smart surfaces,[6] controlled drug release,[7] chromatographic filtration,[8] bioseparation,[9] temperature-triggered optical switches,[10] and biomedical soft materials.[11] Compared with the LCST polymers, the UCST polymers have been less studied. Among them, the uncharged UCST polymers based on thermally reversible hydrogen bonding have received more attention because of their good stability in electrolyte solutions.

Until now, several unchanged UCST polymers, including poly(methacrylamide),[12] poly(uracil acrylate),[13,14] poly(*N*-acryloyglycinamide) and its derivatives,[12,15−21] poly(allylamine-*co*-allylurea),[22] poly(L-citrulline-*co*-ornithine),[23] poly((meth)acrylamide-*co*-*N*-acetylacrylamide),[23] and poly(acrylamide-*co*-acrylonitrile) (P(AAm-*co*-AN)),[12] have been reported. Very recently, Seuring and Agarwal synthesized P(AAm-*co*-AN) by a simple random radical copolymerization of acrylamide (AAm) and acrylonitrile (AN) monomers, which shows sharp and tunable UCST in both water and electrolyte solutions with little hysteresis between cooling and heating cycles.[12] Because of these advantages, P(AAm-*co*-AN) has got a wide range of concerns in academic studies and in applications. Zhao and co-workers have first prepared three amphiphilic diblock copolymer micelles based on uncharged P(AAm-*co*-AN) by reversible addition−fragmentation chain-transfer (RAFT) polymerization with reversible thermoresponsive behaviors in physiological medium.[24] In addition, they also have incorporated either acrylic acid or 4-vinylpyridine

Received: December 16, 2017
Revised: January 27, 2018
Published: February 11, 2018

DOI: 10.1021/acs.langmuir.7b04255
Langmuir 2018, 34, 3058−3067

Scheme 1. Synthesis of the Macroinitiator and HBPO-*star*-P(AAm-*co*-AN)

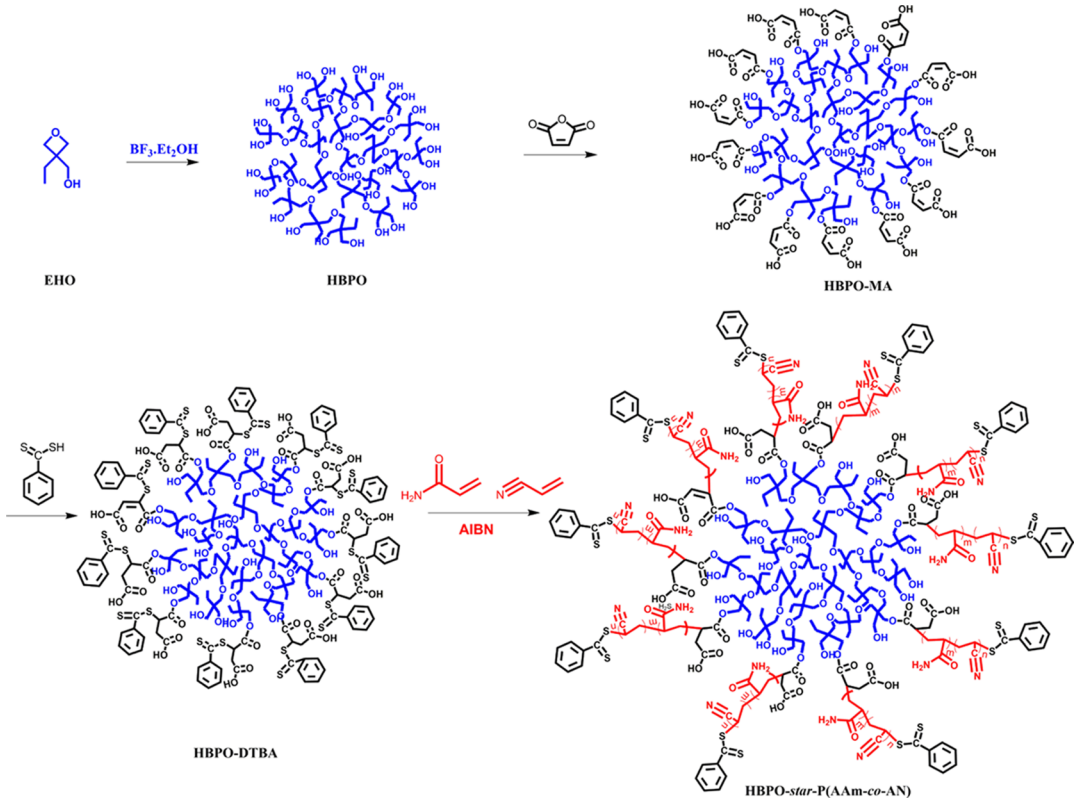

comonomer units into P(AAm-*co*-AN) to obtain the ultrasensitive pH-induced UCST shift.[25] Agarwal and co-workers have reported that P(AAm-*co*-AN) could be cross-linked by UV light to prepare thermophilic hydrogel films and fibers and these hydrogels showed promising applications in the design of microactuators.[26] Li and co-workers have modulated an antitumor drug delivery system by the amphiphilic P(AAm-*co*-AN)-*g*-PEG polymeric micelles with a UCST of 43 °C.[27] Despite the progress, the reported uncharged UCST polymers are mainly focused on linear or brush structures, and the polymer topological structures should be greatly extended.

The demixing behavior of the thermoresponsive polymer is affected by the polymer architecture.[28] Hyperbranched polymers are regarded as a significant sort of functional polymers that not only could be easily fabricated by a one-pot method but also have the special advantages of a large number of terminal functional groups, better solubility, and lower viscosity.[29−31] In our previous works, we found that hyperbranched polymers are excellent polymer precursors in self-assembly and have obtained various supramolecular structures in all scales and dimensions.[32−37] Herein, we report the first UCST polymers with a hyperbranched topological structure. It was found that the hyperbranched structure has a pronounced effect on the UCST transition and the transition mechanism.

The hyperbranched UCST polymer presented here has a hydrophobic hyperbranched poly[3-ethyl-3-(hydroxymethyl)-oxetane] (HBPO) core and many P(AAm-*co*-AN) arms, named as HBPO-*star*-P(AAm-*co*-AN), which were synthesized by the RAFT polymerization of AAm and AN monomers from the HBPO macroinitiator. The obtained HBPO-*star*-P(AAm-*co*-AN)s displayed sharp and tunable UCST transitions in water and electrolyte solution. The UCST could be adjusted not only by the AN content which is the same with the linear polymers but also by the arm length. Most interestingly, a small change of AN content can lead to a large change of UCST for HBPO-*star*-P(AAm-*co*-AN)s because of the amplification effect of the hyperbranched topological structure. In addition, a special UCST transition mechanism was also disclosed for this hyperbranched copolymer.

2. EXPERIMENTAL SECTION

2.1. Materials. HBPO was prepared as the method reported in our previous paper.[32] The structure and synthesis process are shown in Scheme 1. Maleic anhydride (MA, >99%, TCI Reagent Co. Ltd) was recrystallized from toluene and hexane in 6:1 (v/v). Dithiobenzoic acid (DTBA) was synthesized according to the method described by Bai et al.[38] AAm (>98%, TCI Reagent Co. Ltd) was recrystallized from chloroform twice to remove the inhibitor. AN (A.R. grade, Shanghai Chemical Reagent Co. Ltd) was distilled under reduced pressure prior to use. 2,2′-Azobis(2-methylpropionitrile) (AIBN, 95%, Shanghai First Reagent Co. Ltd) was purified by recrystallization twice from ethanol. Tetrahydrofuran (THF, A.R. grade, Shanghai Chemical Reagent Co. Ltd) was refluxed with sodium wires on heating and then distilled under constant pressure. *N*,*N*-Dimethylformamide (DMF) and dimethyl sulfoxide (DMSO) were distilled under reduced pressure prior to use.

2.2. Instrumentation and Measurements. ^{1}H NMR spectra were recorded on a Varian Mercury Plus 400 MHz spectrometer using deuterated DMSO (d_6-DMSO) as the solvent at 80 °C. The variable temperature ^{1}H NMR spectra were recorded in D_2O at different temperatures, and each thermal equilibrium time was 10 min before taking the spectra. The molecular weight and polydispersity of products were measured by size exclusion chromatography (SEC) on a PerkinElmer Series 200 system at 40 °C using DMF as the eluent and poly(methyl methacrylate) as the standard. For the measurements of temperature-responsive phase transition behaviors of copolymers in water and phosphate-buffered solution, a GBC Cintra 10e UV−vis spectrophotometer was equipped by monitoring the transmittance of a 500 nm light beam at a constant cooling and heating rate of 1 °C/min.

DOI: 10.1021/acs.langmuir.7b04255
Langmuir 2018, 34, 3058−3067

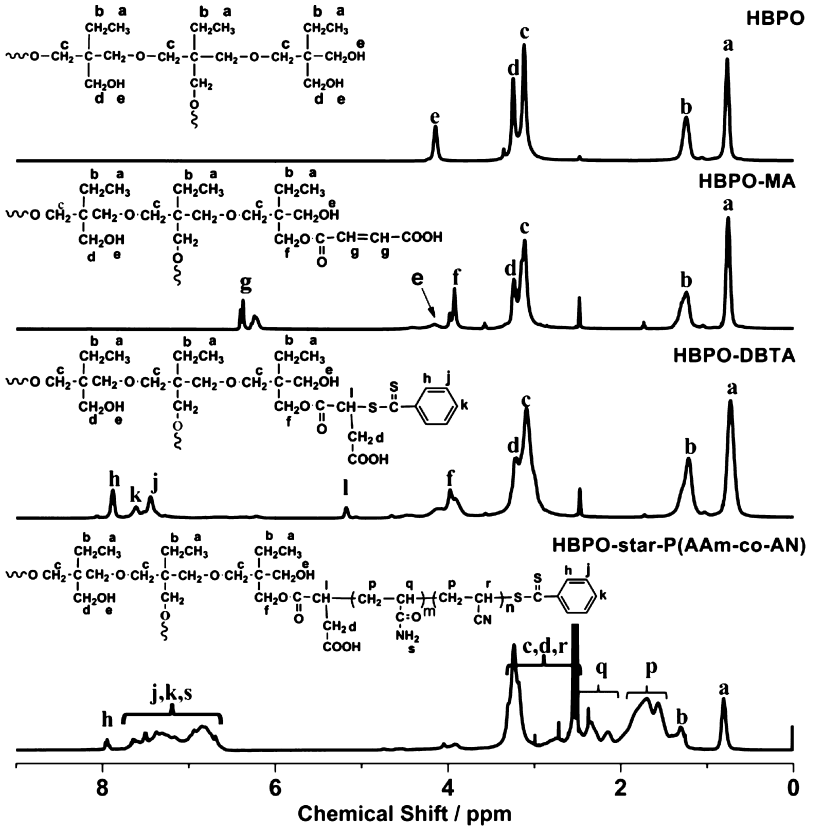

Figure 1. ^{1}H NMR spectra of HBPO, HBPO−MA, HBPO−DBTA, and HBPO-*star*-P(AAm-*co*-AN).

Transmission electron microscopy (TEM) measurements were performed with a JEOL JEM-100CXII instrument at 200 kV. The samples were prepared by depositing a drop of the polymer solution onto copper grids coated with carbon, followed by the addition of one drop of phosphotungstic acid aqueous solution (2 mg/mL, pH = 7) to stain the assemblies, and then the excess solution was removed by a piece of filter paper after 10 min. Finally, the sample was dried at room temperature overnight. Dynamic light scattering (DLS) measurements were performed on Malvern Zetasizer NanoS with 633 nm laser at a scattering angle of 90°. Infrared spectroscopy (IR) was recorded on a PerkinElmer Spectrum 100 FITR spectrometer at 20 °C. The samples were added to KBr and compacted into KBr crystal wafers before the measurement. A series of known-content mixtures of polyacrylamide and polyacrylonitrile homopolymer were measured by IR to obtain a calibration curve that was used to determine the copolymer composition.[12]

2.3. Synthesis of Carboxyl-Group-Terminated HBPO (HBPO−MA). HBPO (2.2 g, 0.63 mmol) was dissolved in 80 mL of anhydrous DMF, followed by the addition of MA (6.8 g, 69.34 mmol). The mixture was stirred at 70 °C for 24 h. After most of the solvent was evaporated under reduced pressure, the residue was diluted with THF. Then, the solution was added dropwise to petroleum ether (60−90 °C) to remove the unreacted MA, and the precipitation was proceeded twice additionally. The obtained HBPO−MA was dried in a vacuum oven at 40 °C for 24 h (yield 45%).

2.4. Synthesis of a Hyperbranched RAFT Agent (HBPO−DTBA). A 100 mL round flask was charged with HBPO−MA (2 g, 0.38 mmol), DTBA (5.3 g, 34.41 mmol) (^{1}H and ^{13}C NMR spectra are shown in Figure S1), and 70 mL dried THF. The mixture was degassed by three freeze−pump−thaw cycles and then heated to 60 °C for 24 h to proceed the addition reaction between DTBA and the double bond of HBPO−MA. The mixture was precipitated into petroleum ether (60−90 °C) three times to completely remove the uncreated DTBA. The light red hyperbranched RAFT agent was obtained by drying in a vacuum oven at 40 °C for 24 h (yield 67%).

2.5. Synthesis of an Uncharged Hyperbranched UCST Copolymer (HBPO-*star*-P(AAm-*co*-AN)). As an example, the synthesis of HBPO-*star*-P(AAm-*co*-AN) with an AN content 24 mol % was conducted as follows. HBPO−DTBA (100 mg, 0.013 mmol) and AAm (1.62 g, 22.8 mmol) were weighted into a 50 mL flask and dissolved in 10 mL distilled DMSO. The reaction mixture was degassed by three freeze−pump−thaw cycles. Then, the initiator AIBN (5 mg, 0.030 mmol) was dissolved into AN (381 mg, 7.2 mmol), and the solution was injected into the flask. The flask was immersed into an oil bath at 70 °C with stirring to proceed polymerization. After the reaction for 24 h, the flask was placed into liquid nitrogen and exposed to air under room temperature. The reaction mixture was precipitated in a 10-fold excess volume of methanol and centrifuged (20 min, 9000 rpm) to get the hyperbranched polymer. This process was repeated three times. The unchanged UCST copolymer HBPO-*star*-P(AAm-*co*-AN) was obtained by drying in a vacuum oven at 40 °C for 24 h. The yield was between 84 and 91% for all reactions.

3. RESULTS AND DISCUSSION

3.1. Characterizations of HBPO-*star*-P(AAm-*co*-AN)s. A typical synthesis route of HBPO-*star*-P(AAm-*co*-AN) is shown in Scheme 1. HBPO was obtained through the cationic ring-opening polymerization of EHO monomers, and then HBPO was reacted with MA to get HBPO−MA. HBPO−MA was further changed into the RAFT macroinitiator of HBPO−DBTA through the terminal modification with DTBA. The final product of HBPO-*star*-P(AAm-*co*-AN) was obtained by the RAFT graft polymerization of monomers AM and AN from HBPO−DBTA. The ^{1}H NMR spectra of HBPO, HBPO−MA, HBPO−DTBA, and typical HBPO-*star*-P(AAm-*co*-AN) samples with assignments are shown in Figure 1. The new signals at 3.9 and 6.2−6.5 ppm that were respectively attributed to the ester methylene (peak f) and double bond (peak g) from the

DOI: 10.1021/acs.langmuir.7b04255
Langmuir 2018, 34, 3058−3067

Table 1. Summary of the Characterization of the HBPO-*star*-P(AAm-*co*-AN) Copolymer

sample number	hyperbranched copolymer, HBPO-*star*-P(AAm_m-*co*-AN_n)	AN in feed[a] (mol %)	AN content in arms[b] (mol %)	arm length[c]	M_n[d] (g/mol)	PDI[d]	M_n[e] (g/mol)	cloud point (°C)[f] cooling	cloud point (°C)[f] heating
P1	HBPO-*star*-P(AAm_{22}-*co*-AN_6)	24.0	23.1	28	22 800	1.50	40 184	33.2	42.8
P2	HBPO-*star*-P(AAm_{21}-*co*-AN_7)	26.5	26.3	28	29 800	1.48	39 874	45.7	55.3
P3	HBPO-*star*-P(AAm_{20}-*co*-AN_8)	27.4	27.2	28	23 200	1.53	39 688	50.4	59.1
P4	HBPO-*star*-P(AAm_{20}-*co*-AN_8)	29.2	29.0	28	32 600	1.58	39 564	65.2	72.6
P5	HBPO-*star*-P(AAm_{21}-*co*-AN_9)	29.2	29.1	30	33 800	1.59	41 257	50.1	63.4
P6	HBPO-*star*-P(AAm_{28}-*co*-AN_{11})	29.2	29.1	39	36 900	1.57	52 102	43.8	53.8
P7	HBPO-*star*-P(AAm_{59}-*co*-AN_{25})	29.2	29.0	84	48 700	1.60	101 998	39.6	50.6

[a]AN content in all two monomers. [b]AN content in the arms of HBPO-*star*-P(AAm-*co*-AN) copolymers and the HBPO core is not taken into calculation. Determined by IR spectroscopy. [c]Calculated by ^{1}H NMR in d_6-DMSO. Arm length means the total DP of AAm and AN units in each arm (DParm) were determined by the integral ratio of peak p to peak h. [d]Determined by SEC. [e]Determined by ^{1}H NMR and calculated by eq 1. [f]Cloud point was defined as the temperature where the transmission had fallen to 50%, and the aqueous concentration was 10 mg/mL.

MA group appeared in the spectrum of HBPO−MA, which confirmed that HBPO was successfully functionalized by the esterification reaction with MA. The conversion of hydroxyl groups was obtained by calculating the integral area of ester methylene (peak f) and hydroxyl groups (peak e) as the formula: $f/(2e + f)$. The result shows a functionalization efficiency of 57%. After the addition reaction of HBPO−MA with DTBA, the signals of double bond (peak g) disappeared and the new signals at 7−8 ppm (peak h, k, j) assigned to the aromatic protons appeared. The above results confirm that the macromolecular RAFT agent HBPO−DTBA was successfully prepared and that the addition efficiency of HBPO−MA with DTBA was 100%. In the typical ^{1}H NMR spectrum of HBPO-*star*-P(AAm-*co*-AN), both HBPO (peak a, b) and P(AAm-*co*-AN) (peak p, q, h, j, k, s) signals can be found obviously and the signal of −CH−SCS− groups (peak l) disappeared completely. These results indicate that the monomers were successfully inserted into the −C−SCS− bond and that HBPO-*star*-P(AAm-*co*-AN)s were prepared successfully. In addition, HBPO-*star*-P(AAm-*co*-AN) was further employed as the macrochain-transfer agent to copolymerize the styrene. The ^{1}H NMR and SEC results (see in Figures S2 and S3) showed that polystyrene was successfully grafted onto the HBPO-*star*-P(AAm-*co*-AN) to get HBPO-*star*-(P(AAm-*co*-AN)-*b*-PS), which further proved the controlled properties of the polymerization process used here.

Herein, seven HBPO-*star*-P(AAm-*co*-AN) copolymer samples with the same HBPO core but different P(AAm-*co*-AN) arms (P1−P7) were synthesized. To determine the copolymer composition, the IR calibration curve (see Figure S4) was used to obtain the AN content in polymer, and the results are listed in Table 1. The results show that the AN content in polymers is close to the feed ratio of AN/AAm in the monomer mixture, which indicates that the RAFT polymerizations are well-controlled. The average arm length, meaning the total degree of polymerization (DP) of AAm and AN units in each arm (DP_{arm}), can be determined by the integral ratio of peak p (methylene group in all monomer units) to peak h (two aromatic protons of hyperbranched copolymer terminal groups) (listed in Table 1). Then, the average DP of AN in each arm was calculated by multiplying the arm length by the AN content in polymers. The final copolymer compositions are summarized in Table 1. According to the above results, all the polymers can be divided into two series, series A of polymers with varied AN content but almost the same arm length (P1−P4, DP_{arm} = 28) and series B of polymers with varied arm length but almost the same AN content (P4−P7, AN content = 29.0−29.1%). It can be seen from the molecular weight measured by SEC (see Figure S5) that there is no obvious variation trend in the molecular weight of HBPO-*star*-P(AAm-*co*-AN) samples (P1−P4) when the arm length is close. However, the molecular weight of HBPO-*star*-P(AAm-*co*-AN) samples (P4−P7) increased sequentially with the increase of arm length, which further confirms the successful copolymerization of the two monomers onto the HBPO cores. The hydrodynamic volume of hyperbranched polymers is smaller than that of linear analogues;[39] in addition, the molecular weight of P(AAm-*co*-AN)s measured by SEC is not certain because the massive functional groups make the polymers easy to be absorbed to the surface SEC columns. Thus, the SEC result of HBPO-*star*-P(AAm-*co*-AN) might be smaller than the truth. Thus, the M_n values of all samples were also calculated in eq 1 (listed in Table 1), according to the structural characterization results obtained by ^{1}H NMR and IR spectroscopy. It should be mentioned that all the copolymers (P1−P7) have the same HBPO core (degree of branch: 40%) (see Figure S6) and that the M_n value of the HBPO core was detected by SEC (M_n: 3500, PDI: 2.36) (see Figure S7). The molecular weight distribution of HBPO precursors is relatively high; however, after copolymerization with AAm and AN, the polydispersity index of HBPO-*star*-P(AAm-*co*-AN) copolymers decreases (<1.60) because of the advantage of RAFT polymerization.

$$M_n = M_{(HBPO)} + M_{(HBPO)}/116 \times 57\% \times (253 + M_{AAm} \times m + M_{AN} \times n) \quad (1)$$

3.2. Thermoresponsibility of the HBPO-*star*-P(AAm-*co*-AN) Solution. All aqueous solutions of the HBPO-*star*-P(AAm-*co*-AN) copolymers display visible UCST temperature-responsive behaviors. A typical solution property of the copolymer (P4) during cooling is shown in Figure 2. The copolymer aqueous solution was pale pink, clear, and transparent at 80 °C (Figure 2a). However, when the aqueous solution was cooled to room temperature, it turned into a pink opaque suspension (Figure 2b). Finally, the copolymers precipitated from water onto the bottom of the vessel after keeping in the room temperature for 1 month (gray arrow in Figure 2c), and the solution showed obvious stratification. The temperature-responsive property of the copolymer solution is

DOI: 10.1021/acs.langmuir.7b04255
Langmuir 2018, 34, 3058−3067

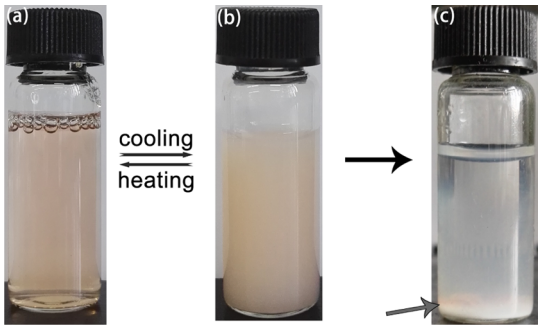

Figure 2. HBPO-*star*-P(AAm-*co*-AN) solution: (a) at 80 °C; (b) at room temperature; and (c) at room temperature for 1 month.

reversible. When the turbid solution in the room temperature was heated up to 80 °C again, it could change into a clear solution again, so was the reverse process.

3.3. Effect of the Molecular Structure on the UCST Transition. To study the effect of the molecular structure on UCST transition, two series of HBPO-*star*-P(AAm-*co*-AN)s with variable AN content (series A, P1−P4) and variable arm length (series B, P4−P7) were detected by variable temperature UV−vis spectrometry. All the experiments were directly conducted in aqueous solutions with a constant polymer concentration of 10 mg/mL and a constant cooling rate of 1 °C/min. The cloud point is where the transmittance decreased to 50%.

3.3.1. AN Content Effect. Figure 3a shows the transmittance−temperature curves of series A of HBPO-*star*-P(AAm-*co*-AN)s with variable AN content but the same arm length. The transmittance decreases sharply in all solutions at a specific temperature on cooling, indicating a UCST transition. In addition, comparing the transmittance curves with one another, it is evident that the copolymer having a higher AN content possesses a higher cloud point in water (Figure 3b) which is the same with the linear copolymer P(AAm-*co*-AN).[12]

In addition, the cloud point of the hyperbranched copolymer varies greatly from 33.2 to 65.2 °C with little change of AN content (23.1−29.0%), which indicates that the hyperbranched topological structure makes an amplification effect on the UCST transition.[40] Besides, it can be seen from Figure 3a that the maximum transmittance of the copolymer aqueous solution is similar when the arm length of the copolymer is close.

3.3.2. Arm Length Effect. Figure 3c shows the transmittance−temperature curves of series B of HBPO-*star*-P(AAm-*co*-AN)s with variable arm length but the same AN content. Similar to series A, all polymers in series B show sharp UCST transitions in water, and the cloud point decreases from 65.2 to 39.6 °C with the increase of the DP_{arm} from 28 to 84 (Figure 3d). In addition, the solutions of copolymers with different arm lengths have different maximum transmittances. With the increase of the arm length, the maximum transmittance of the copolymer aqueous solution is also increased. Combining the results of the previous A series (the same arm length and the same maximum transmittance), we could conclude that the arm length of the copolymer determines the maximum transmittance of the copolymer aqueous solution.

3.4. Properties of UCST Transition. *3.4.1. Effect of Solution Concentration.* To investigate the effect of concentration on the UCST transition, the temperature dependence of optical transmittance of P7 aqueous solutions with three concentrations (2.5, 5, and 10 mg/mL) on cooling was measured. As shown in Figure 4a, the cloud point temperature was 27.6, 35.5, and 39.6 °C at the concentration of 2.5, 5, and 10 mg/mL, respectively. Evidently, the cloud point decreased with solution dilution. In addition, the broadening of the UCST transition was evident at the diluted solution of 2.5 mg/mL. The UCST transition of linear P(AAm-*co*-AN) also has such a concentration dependence.[12]

3.4.2. Effect of Electrolyte and Salt Concentration. Three typical temperature dependences of the transmittance of the copolymers in H_2O or PBS at a concentration of 10 mg/mL on cooling (1 °C/min) are displayed in Figure 4b. As seen from

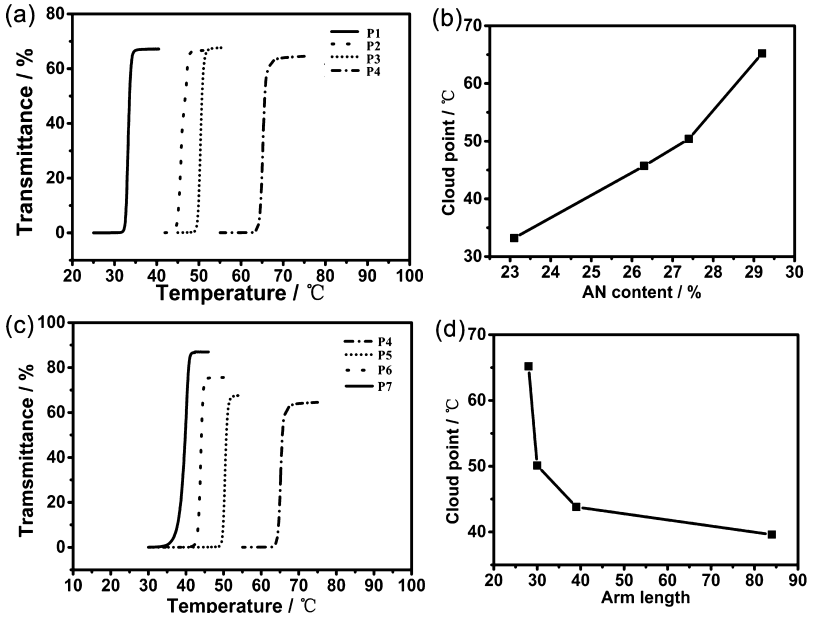

Figure 3. Effect of the molecular structure on the UCST transition. (a) Temperature dependence of optical transmittance at 500 nm for the aqueous solution of series A. (b) Dependence of the cloud point on the AN content for the copolymer in series A. (c) Temperature dependence of optical transmittance at 500 nm for the aqueous solution of series B. (d) Dependence of the cloud point on the arm length for the copolymer in series B.

DOI: 10.1021/acs.langmuir.7b04255
Langmuir 2018, 34, 3058−3067

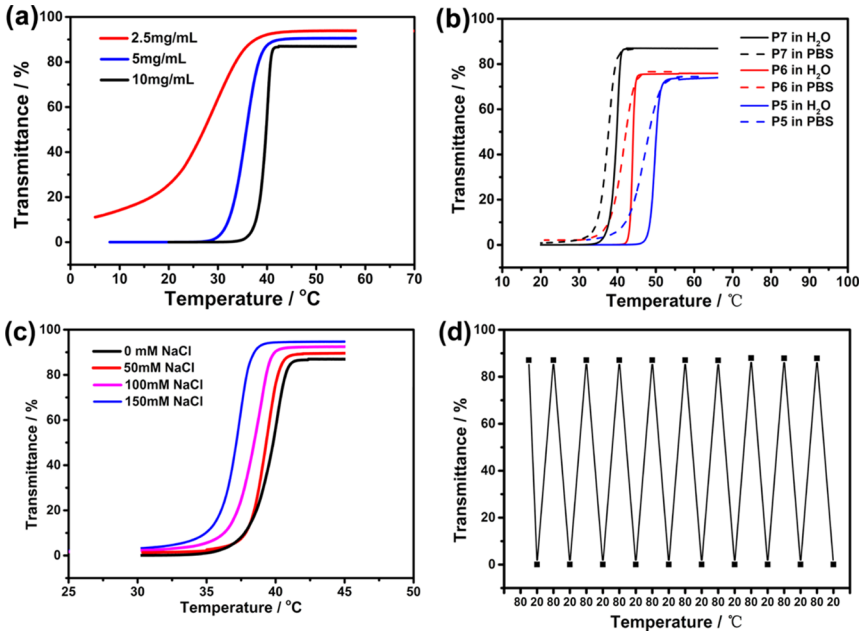

Figure 4. Characterizations of the UCST transition. (a) Temperature dependence of optical transmittance of P7 aqueous solutions with various concentrations on cooling. (b) Temperature dependence of optical transmittance of P5, P6, and P7 solutions in H_2O and PBS buffer on cooling. (c) Temperature dependence of optical transmittance of P7 aqueous solutions with varied NaCl concentrations on cooling. (d) Reversible changes of optical transmittance against temperature fluctuation for P7 aqueous solution.

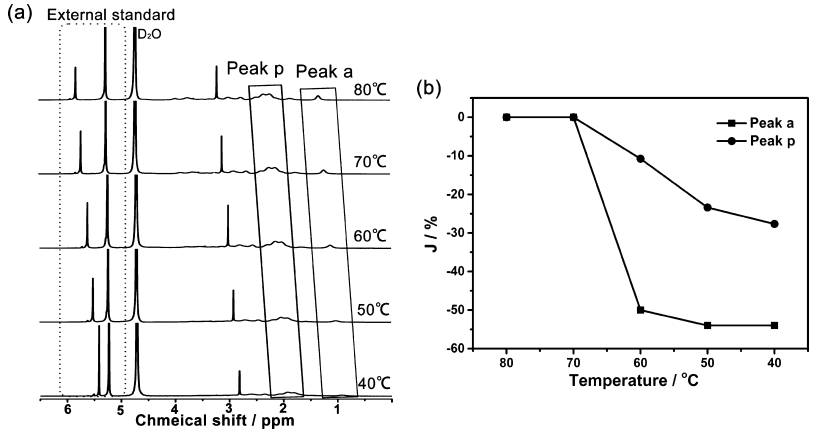

Figure 5. Molecular-level characterization of the UCST transition. (a) ^{1}H NMR spectra of P4 in D_2O (10 mg/mL) conducted at 80, 70, 60, 50, and 40 °C. (b) Intensity change ratio (J) of the two peaks in ^{1}H NMR spectra on cooling.

Figure 4b, the cloud point on cooling in PBS was similar to that measured in water, which was lower only by 2−3 °C. In addition, the UCST transition in PBS buffer is slightly insensitive than that in H_2O, but it still shows a sharp UCST transition. Furthermore, the effect of salt concentration on the UCST transition was also investigated. The temperature dependences of optical transmittance of P7 aqueous solutions with four NaCl concentrations (0, 50, 100, and 150 mM) on cooling were measured. The results as shown in Figure 4c indicated that the cloud point was slightly decreased from 39.6 to 37.1 °C with the addition of NaCl. As we know, for the zwitterionic UCST polymers, the cloud points should decrease several tens of degree with comparable NaCl concentration.[41] Thus, the salt concentration dependence on the UCST transitions for HBPO-*star*-P(AAm-*co*-AN) is fairly small, which is very similar to that of linear P(AAm-*co*-AN).[12,42] Thus, we believed that similar to the linear P(AAm-*co*-AN), strong hydrogen bonds play an important role in the UCST phase transition of HBPO-*star*-P(AAm-*co*-AN), which is far different from the charge−charge interactions for zwitterionic systems.[41]

3.4.3. Reversibility of the UCST Transition. The temperature-responsive UCST transition of HBPO-*star*-P(AAm-*co*-AN) is reversible and stable. Ten consecutives of optical transmittance measurements for P7 solution between 20 and 80 °C in water are displayed in Figure 4d. At 80 °C, above the UCST, the P7 solution showed a high transmittance of 89% and it became cloudy with a low transmittance of nearly 0% at 20 °C. The polymer solution underwent the very similar transmittance changes in the subsequent heating and cooling cycles. It indicates that the UCST transition of the HBPO-*star*-P(AAm-*co*-AN) solution is reversible and stable.

3.5. Molecular-Level Investigation of the UCST Transition. A quantitative variable temperature ^{1}H NMR analysis was performed to investigate the molecular mechanism of the UCST transition of the HBPO-*star*-P(AAm-*co*-AN)

DOI: 10.1021/acs.langmuir.7b04255
Langmuir 2018, 34, 3058−3067

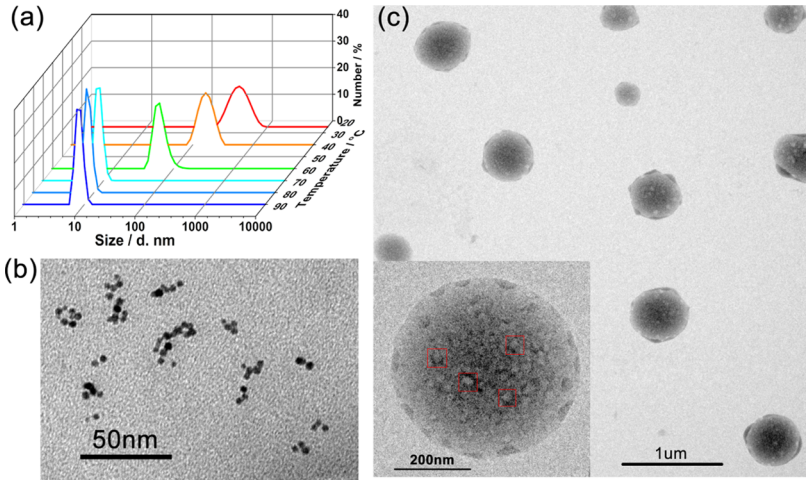

Figure 6. Self-assembled structure transition during the UCST transition. (a) DLS plots of the micellar solution of P4 on cooling. (b) TEM images of the micelles at 80 °C. (c) TEM images of the micelles at 25 °C.

copolymer. Glyoxylic acid was added as the external standard, and its signal (peak 5.2 ppm, HCO−) was kept in the same intensity in the ^{1}H NMR spectra. Signals of D_2O were kept in the same position (4.79 ppm) for calibration. Figure 5a shows typical variable temperature ^{1}H NMR spectra from the P4 sample. Peak p is attributed to $-CH_2-$ groups in P(AAm-*co*-AN) arms, whereas peak a is attributed to the $-CH_3$ groups from the HBPO core. These two peaks were respectively selected for the quantitative analyses.

To quantitatively explore the mobility change of copolymers in the aqueous solution with decreasing temperature, the intensity decrease ratio (J) was calculated by comparing the integrated area of the proton peak at a lower temperature (A_T) to that at 80 °C (A_{80}), and the calculation equation is $J = (A_T - A_{80})/A_{80} \times 100\%$. The results are shown in Figure 5b. As for peak p, the J_p undergoes a sigmoid transition with the decrease of temperature: it was kept constant before 70 °C and then decreased rapidly when the temperature was dropped from 70 to 50 °C. The J_p decreased less when the temperature was reduced from 50 to 40 °C. Evidently, the P(AAm-*co*-AN) arms have underwent a dramatic dehydration at a critical temperature that agrees well with the cloud point (65.2 °C) detected by a UV−vis spectrometer (Figure 3a). Thus, we can draw a conclusion that the UCST transition of HBPO-*star*-P(AAm-*co*-AN)s originates from the dehydration of P(AAm-*co*-AN) arms. As for peak a, the J_a also undergoes a sigmoid transition with decreasing temperature. In addition, the J_a has the same transition temperature with peak p, and the transition is more apparent at the critical temperature than that of peak p. These results indicate that the hydrophobic HBPO core adopted a tightly packing model to quickly avoid the unfavorable content with water and aggregated into solidlike micelle core domains with the decrease of temperature, and so, they can hardly be detected by NMR at 40 °C. Thus, it can be deduced that the UCST phase transition of HBPO-*star*-P(AAm-*co*-AN)s is highly related not only with the dehydration of P(AAm-*co*-AN) arms upon cooling but also with the collapse of the HBPO cores. As mentioned above, HBPO-*star*-P(AAm-*co*-AN)s show unusual broad changes of phase transition temperature with a small adjustment of the AN content, which is attributed to the amplification effect of the hyperbranched topological structure. The result as shown in Figure 5b did prove the existence of such an amplification effect related with the conformation changes of the hyperbranched cores.

3.6. Self-Assembly Behaviors during the UCST Transition. Combined with the results of molecular-level investigation, we proposed that some self-assembly process might happen during the UCST transition of the HBPO-*star*-P(AAm-*co*-AN)s. To verify the proposal, DLS and TEM were used to characterize the assembled structures of HBPO-*star*-P(AAm-*co*-AN) on cooling. Figure 6a shows the variable temperature DLS results on the cooling of the P4 aqueous solution from 90 to 25 °C. At the high temperature (90−70 °C), HBPO-*star*-P(AAm-*co*-AN) dissolved in water in the unimolecular micelle state with a hydrodynamic diameter (D_h) of around 8.3 nm. Upon further cooling to 60 °C, the D_h increased to about 75 nm, which indicated that the UCST phase transition of copolymers occurred and that large particles were formed. When the temperature decreased to 25 °C, the D_h further increased to about 350 nm, indicating the further aggregation of particles. The TEM observation also confirmed the aggregate formation during the UCST transition (Figure 6b,c). As shown in Figure 6b, at 80 °C, HBPO-*star*-P(AAm-*co*-AN) presented the unimolecular micelle with the average size of around 6.3 nm. When the temperature decreased to 25 °C, large spherical micelles with the average size of around 400 nm were observed.

3.7. UCST Transition Mechanism. According to our previous report, the large multimolecular micelles (>100 nm) from hyperbranched multiarm copolymers should be a kind of multimicelle aggregates (MMAs), which can be divided into the unimolecular micelle aggregate (UMA) or small micelle aggregate (SMA) mechanisms.[40−45] The UMA micelles are constructed by the secondary aggregation of unimolecular micelles (generally around 10 nm), whereas the SMA micelles are obtained through the secondary aggregation of small micelles (generally around 20 nm).[43] In the enlarged TEM image (inset of Figure 6c), many small spherical building blocks could be discerned clearly inside the large spherical micelles. The size of these small building blocks was around 20 nm (labeled in red square), which is almost the double size of unimolecular micelles (D_h = 8.3 nm). Thus, we believed the building blocks in the large micelles were the microphase-separated small micelles, and HBPO-*star*-P(AAm-*co*-AN)

DOI: 10.1021/acs.langmuir.7b04255
Langmuir 2018, 34, 3058−3067

copolymers should obey the SMA mechanism during the UCST transition.[43]

The UCST transition mechanism was proposed in Figure 7. At the temperature above the UCST, HBPO-*star*-P(AAm-*co*-AN)s form the unimolecular micelles around 10 nm and the P(AAm-*co*-AN) chains in the micelle corona (in red) are stretching out because of the hydrogen bond between the amide group and water molecules. When the micelle solution is cooled to the critical temperature, the amide−water hydrogen bonds are partly broken up, which leads to the hydrophilic/hydrophobic misbalance of the polymer micelles. To reach a new hydrophilic/hydrophobic balance, the spherical dendritic multiarm copolymers further aggregate into small micelles, in which a spherical-to-cone microphase separation with self-segregated hydrophilic arms and hydrophobic cores inside the micelle occurs.[43] In this microphase-separated small micelle, the diameter should be equal to the length of two HBPO-*star*-P(AAm-*co*-AN) polymers (around 20 nm). With the further decrease of the temperature, the microphase-separated small micelles are not stable and would further shrink because of the continuous dehydration process. Finally, the shrunken small micelles will further aggregate into large SMAs around 400 nm to reach the final equilibrium of the UCST transition.

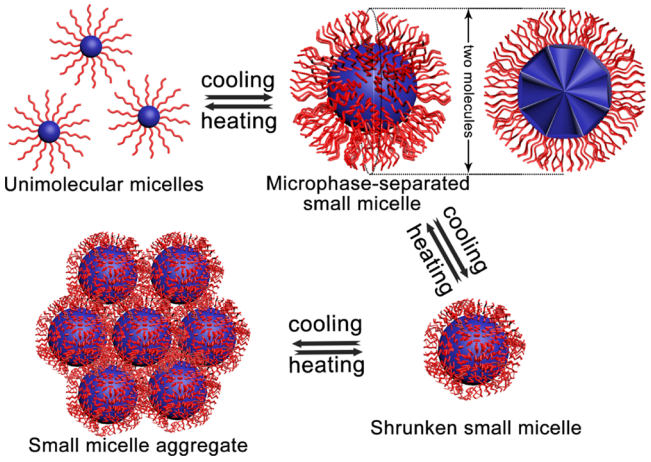

Figure 7. Proposed UCST transition mechanism for HBPO-*star*-P(AAm-*co*-AN)s.

3.8. Applications of the UCST Transition Mechanism. *3.8.1. Explanations for the Effect of Arm Length on the Cloud Point.* Herein, as shown in Figure 3c,d, it was found that the cloud points of HBPO-*star*-P(AAm-*co*-AN)s were highly dependent on the arm length, which could be understood readily according to the mechanism proposed in Figure 7. The HBPO-*star*-P(AAm-*co*-AN) unimolecular micelle having longer P(AAm-*co*-AN) arms possesses much more hydrated water around the micelle shell, which provides a better solubility of the unimolecular micelle. Thus, during the cooling cycle, lower temperature is needed to destroy the hydrated water to form SMAs, leading to a decrease of the cloud point with the increase of the arm length.

3.8.2. Explanations for the Concentration Dependence. Figure 7 can also be used to explain the strong concentration dependence of the cloud point of HBPO-*star*-P(AAm-*co*-AN)s as shown in Figure 4a. In diluted solution, the unimolecular or small micelles could not "find" each other as quickly as in concentrated solution, and thus, they could not further aggregate into large micelles rapidly. Thus, the optical transmittance of the diluted solution decreased more slowly, and a lower temperature was needed to trigger the aggregation of small micelles into large micelles during cooling. Therefore, it is the slow micelle aggregate process that causes the lower cloud point and broader UCST transition on the diluted solution of HBPO-*star*-P(AAm-*co*-AN)s.

3.8.3. Explanations for the Hysteresis. As we know, P(AAm-*co*-AN) generally shows a sharp UCST with little hysteresis between cooling and heating cycles, only 1−2 °C.[12] However, HBPO-*star*-P(AAm-*co*-AN) exhibits the UCST transition with a large hysteresis between cooling and heating cycles (see Figure S8), and the phase transition on heating is much slower. This proposed mechanism based on the micelle self-assembly in Figure 7 can well explain the hysteresis. In the heating process, the large SMA micelles formed in the previous cooling cycle should disassemble into unimolecular micelles. As shown in Figure 7, there should be two steps of disassembly. First, the microphase-separated small micelles that are tightly packed in the SMA micelles should be disassembled, and second, the small micelles should further disassemble into unimolecular micelles. Therefore, it is the slow disassembly dynamics that leads to the slow UCST transition during heating cycle as well as the obvious hysteresis between cooling and heating cycles.

4. CONCLUSIONS

In conclusion, the work displayed the first highly branched temperature-responsive polymers with the UCST phase transition. The polymer has a hyperbranched HBPO core and many linear P(AAm-*co*-AN) arms, which shows sharp, reversible, and tunable UCST transition in water and electrolyte solution. The phase transition temperature of copolymers is highly dependent on the AN content and the arm length. Because of the amplification effect of the hyperbranched topological structure, the cloud point of copolymers varied greatly from 33.2 to 65.2 °C with little change of AN content (5.9%). In addition, the cloud point of copolymers decreases with the increase of the arm length. Detailed mechanism investigations indicate that the UCST transition of the thermosensitive copolymer results from the dehydration of P(AAm-*co*-AN) arms and hyperbranched cores as well as the self-assembled structure transformations of the copolymer during cooling cycle. With the decrease in temperature, the thermosensitive copolymer transforms from unimolecular micelles to microphase-separated small micelles and then further assembles into the SMA. The present work has extended the category of UCST polymers from linear to highly branched structures. In addition, the findings presented here will contribute to a fundamental understanding on the relationship between the molecular topology and the UCST transition behaviors.

■ ASSOCIATED CONTENT

Supporting Information

The Supporting Information is available free of charge on the ACS Publications website at DOI: 10.1021/acs.langmuir.7b04255.

Characterization of DTBA, synthesis and characterizations of HBPO-*star*-(P(AAm-*co*-AN)-*b*-PS), determination of AN content in HBPO-*star*-P(AAm-*co*-AN) samples, characterization molecular weight of HBPO-*star*-P(AAm-*co*-AN)s, characterization DB of the HBPO

DOI: 10.1021/acs.langmuir.7b04255
Langmuir 2018, 34, 3058−3067

core, characterization molecular weight of HBPO, and characterization UCST of the HBPO-*star*-P(AAm-*co*-AN)s (PDF)

AUTHOR INFORMATION

Corresponding Author

*E-mail: yfzhou@sjtu.edu.cn.

ORCID

Yongfeng Zhou: 0000-0001-6282-5882

Notes

The authors declare no competing financial interest.

ACKNOWLEDGMENTS

Financial support from the National Natural Science Foundation of China (91527304, 21474062, and 51773115), the Program of Shanghai Subject Chief Scientist (15XD1502400), and the Shanghai Basic Research Project (17JC1403400) is gratefully acknowledged.

REFERENCES

(1) Stuart, M. A. C.; Huck, W. T. S.; Genzer, J.; Müller, M.; Ober, C.; Stamm, M.; Sukhorukov, G. B.; Szleifer, I.; Tsukruk, V. V.; Urban, M.; Winnik, F.; Zauscher, S.; Luzinov, I.; Minko, S. Emerging applications of stimuli-responsive polymer materials. *Nat. Mater.* **2010**, *2*, 101−113.

(2) de Espinosa, L. M.; Meesorn, W.; Moatsou, D.; Weder, C. Bioinspired polymer systems with stimuli-responsive mechanical properties. *Chem. Rev.* **2017**, *117*, 12851−12892.

(3) Roy, D.; Brooks, W. L. A.; Sumerlin, B. S. New directions in thermoresponsive polymers. *Chem. Soc. Rev.* **2013**, *42*, 7214−7243.

(4) Pineda-Contreras, B. A.; Schmalz, H.; Agarwal, S. pH dependent thermoresponsive behavior of acrylamide-acrylonitrile UCST-type copolymers in aqueous media. *Polym. Chem.* **2016**, *7*, 1979−1986.

(5) de las Heras Alarcón, C.; Pennadam, S.; Alexander, C. Stimuliresponsive polymers for biomedical applications. *Chem. Soc. Rev.* **2005**, *34*, 276−285.

(6) Nagase, K.; Kobayashi, J.; Okano, T. Temperature-responsive intelligent interfaces for biomolecular separation and cell sheet engineering. *J. R. Soc., Interface* **2009**, *6*, S293−S309.

(7) Nakayama, M.; Okano, T.; Miyazaki, T.; Kohori, F.; Sakai, K.; Yokoyama, M. Molecular design of biodegradable poymeric micelles for temperature-responsive drug release. *J. Controlled Release* **2006**, *115*, 46−56.

(8) Ayano, E.; Kanazawa, H. Aqueous chromatography system using temprature-responsive polymer-modified. *J. Sep. Sci.* **2006**, *29*, 738−749.

(9) Hoffman, A. S.; Stayton, P. S. Conjugates of stimuli-respinsive polymers and proteins. *Prog. Polym. Sci.* **2007**, *32*, 922−932.

(10) Asher, S. A.; Weissman, J. M.; Sunkura, H. B. Thermally switchable optical devices. U.S. Patent 6,165,389 A, March 10, 2000.

(11) Xu, J.; Luo, S.; Shi, W.; Liu, S. Two-stage collapse of unimolecular micelles with double thermoresponsive coronas. *Langmuir* **2006**, *22*, 989−997.

(12) Seuring, J.; Agarwal, S. First example of a universal and cost-effective approach: polymers with tunable upper critical solution temperature in water and wlectrolyte solution. *Macromolecules* **2012**, *45*, 3910−3918.

(13) Aoki, T.; Nakamura, K.; Sanui, K.; Ogata, N.; Kikuchi, A.; Okano, T.; Sakurai, Y. Temperature-responsive drug release from polymeric hydrogels based on 6-(acryloyloxymethyl) uracil in physiological solution. *Proc. Int. Symp. Controlled Release Bioact. Mater.* **1996**, *23*, 767−768.

(14) Aoki, T.; Nakamura, K.; Sanui, K.; Kikuchi, A.; Okano, T.; Sakurai, Y.; Ogata, N. Adenosine-induced changes of the phase transition of poly (6-(acryloyloxymethyl)uracil) aqueous solution. *Polym. J.* **1999**, *31*, 1185−1188.

(15) Seuring, J.; Bayer, F. M.; Huber, K.; Agarwal, S. Upper Critical solution temperature of poly(N-acryloyl glycinamide) in water: a concealed property. *Macromolecules* **2012**, *45*, 374−384.

(16) Nagaoka, H.; Ohnishi, N.; Eguchi, M. (Chisso Corporation). Thermoresponsive Polymer and Production Method Thereof. U.S. Patent 20,070,203,313 A1, Aug 30, 2007.

(17) Ohnishi, N.; Furukawa, H.; Kataoka, K.; Ueno, K. (National Institute of Advanced Industrial Science and Technology; Chisso Corporation). Polymer Having an Upper Critical Solution Temperature. U.S. patent 7,195,925 B2, March 27, 2007.

(18) Ohnishi, N.; Furukawa, H.; Hideyuki, H.; Wang, J.-M.; Fukusaki, E.; Kataoka, K.; Ueno, K.; Kondo, A. High-efficiency bioaffinity separation of cells and proteins using novel thermoresponsive biotinylated magnetic nanoparticles. *NanoBiotechnology* **2006**, *2*, 43−49.

(19) Seuring, J.; Agarwal, S. Non-ionic homo- and copolymers with H-donor and H-acceptor units with an UCST in water. *Macromol. Chem. Phys.* **2010**, *211*, 2109−2117.

(20) Liu, F.; Seuring, J.; Agarwal, S. Controlled radical polymerization of N-Acryloylglycinamide and UCST-type phase transition of the polymers. *J. Polym. Sci., Part A: Polym. Chem.* **2012**, *50*, 4920−4928.

(21) Eguchi, M.; Ohnishi, N. Aqueous Solution of Polymer Having Upper Critical Solution Temperature, Aqueous Dispersion of Particle Modified with the Polymer and Method of Storing the Same. U.S. Patent 7,976,728 B2, July 12, 2011.

(22) Shimada, N.; Ino, H.; Maie, K.; Nakayama, M.; Kano, A.; Maruyama, A. Ureido-derivatized polymers based on both poly(allylurea) and poly(L-citrulline) exhibit UCST-type phase transition behavior under physiologically relevant conditions. *Biomacromolecules* **2011**, *12*, 3418−3422.

(23) Ohnishi, N.; Aoshima, K.; Kataoka, K.; Ueno, K. (Agency of Industrial Science and Technology MITI; Japan Chemical Innovation Institute), EP 0922715 A2, 1999.

(24) Zhang, H.; Tong, X.; Zhao, Y. Diverse thermoresponsive behaviors of uncharged UCST block copolymer micelles in physiological medium. *Langmuir* **2014**, *30*, 11433−11441.

(25) Zhang, H.; Guo, S.; Fan, W.; Zhao, Y. Ultrasensitive pH-induced water solubility switch using UCST polymers. *Macromolecules* **2016**, *49*, 1424−1433.

(26) Liu, F.; Jiang, S.; Ionov, L.; Agarwal, S. Thermophilic films and fibers from photo cross-linkable UCST-type polymers. *Polym. Chem.* **2015**, *6*, 2769−2776.

(27) Li, W.; Huang, L.; Ying, X.; Jian, Y.; Hong, Y.; Hu, F.; Du, Y. Antitumor drug delivery modulated by a polymeric micelle with an upper critical solution temperature. *Angew. Chem., Int. Ed.* **2015**, *54*, 3126−3131.

(28) Furyk, S.; Zhang, Y.; Ortiz-Acosta, D.; Cremer, P. S.; Bergbreiter, D. E. Effects of end group polarity and molecular weight on the lower critical solution temperature of poly(N-isopropylacrylamide). *J. Polym. Sci., Part A: Polym. Chem.* **2006**, *44*, 1492−1501.

(29) Gao, C.; Yan, D. Hyperbranched polymers: from synthesis and applications. *Prog. Polym. Sci.* **2004**, *29*, 183.

(30) Carlmark, A.; Hawker, C.; Hult, A.; Malkoch, M. New methodologies in the construction of dendritic materials. *Chem. Soc. Rev.* **2009**, *38*, 352−362.

(31) Voit, B. I.; Lederer, A. Hyperbranched and highly branched polymer architectures-synthetic strategies and major characterization aspects. *Chem. Rev.* **2009**, *109*, 5924−5973.

(32) Zhou, Y.; Huang, W.; Liu, J.; Zhu, X.; Yan, D. Self-assembly of hyperbranched polymers and its biomedical application. *Adv. Mater.* **2010**, *22*, 4567−4590.

(33) Zhou, Y.; Yan, D. Supramolecular self-assembly of amphiphilic hyperbranched polymers at all scales and dimensions: progress, characteristics and perspectives. *Chem. Commun.* **2009**, 1172−1188.

(34) Jiang, W.; Zhou, Y.; Yan, D. Hyperbranched polymer vesicles: from self-assembly, characterization, mechanisms, and properties to applications. *Chem. Soc. Rev.* **2015**, *44*, 3874−3889.

DOI: 10.1021/acs.langmuir.7b04255
Langmuir 2018, 34, 3058−3067

(35) Xu, F.-G.; Mai, Y.-Y.; Zhou, Y.-F. Investigation on the effect of water content on the morphology of hyperbranched polymer aggregates in solution through a fluorescence labeling approach. *Acta Polym. Sin.* **2017**, *2*, 274−281.
(36) Qi, M. W.; Huang, W.; Xiao, G. Y.; Zhu, X. Y.; Gao, C.; Zhou, Y. F. Synthesis and self-assembly of hyperbranched polymers. *Acta Polym. Sin.* **2017**, *2*, 214−227.
(37) Hou, Z.-L.; Huang, T.; Cai, C.-Y.; Resheed, T.; Yu, C.-Y.; Zhou, Y.-F.; Yan, D.-Y. Polymer vesicle sensor through the self-assembly of hyperbranched polymeric inoic liquids for the detectin of SO2 derivatives. *Chin. J. Polym. Sci.* **2017**, *35*, 602−610.
(38) Bai, R.-K.; You, Y.-Z.; Pan, C.-Y. Study on controlled free-radical polymerization in the presence of dithiobenzoic acid (DTBA). *Polym. Int.* **2000**, *49*, 898−902.
(39) Atthoff, B.; Trollsås, M.; Claesson, H.; Hedrick, J. L. Poly(lactides) with controlled molecular architecture initiated from hydroxyl functional dendrimers and the effect on the hydrodynamic volume. *Macromol. Chem. Phys.* **1999**, *200*, 1333−1339.
(40) Zhou, Y.; Yan, D.; Dong, W.; Tian, Y. Temperature-responsive phase transition of polymer vesicles: real time morphology observation and molecular mechanism. *J. Phys. Chem. B* **2007**, *111*, 1262−1270.
(41) Zhu, Y.; Noy, J.-M.; Lowe, A. B.; Roth, P. J. The synthesis and aqueous solution properties of sulfobutylbetaine (co)polymers: comparison of synthetic routes and tuneable upper critical solution temperatures. *Polym. Chem.* **2015**, *6*, 5705−5718.
(42) Hou, L.; Wu, P. Understanding the UCST-type transition of P(AAm-*co*-AN) in H_2O and D_2O: dramtic effects of solvent isotopes. *Soft Matter* **2015**, *11*, 7059−7065.
(43) Wang, Y.; Li, B.; Zhou, Y.; Lu, Z.; Yan, D. Dissipative particle dynamics simulation study on the mechanisms of self-assembly of large multimolecular micelles from amphiphilic dendritic multiarm copolymers. *Soft Matter* **2013**, *9*, 3292−3304.
(44) Hong, H.; Mai, Y.; Zhou, Y.; Yan, D.; Cui, J. Self-assembly of large multimolecular micelles from hyperbranched star copolymers. *Macromol. Rapid Commun.* **2007**, *28*, 591−596.
(45) Mai, Y.; Zhou, Y.; Yan, D. Synthesis and size-controllable self-assembly of a novel amphiphilic hyperbranched multiarm copolyether. *Macromolecules* **2005**, *38*, 8679−8686.

DOI: 10.1021/acs.langmuir.7b04255
Langmuir 2018, 34, 3058−3067